arXiv:1408.3802v1 [q-bio.MN] 17 Aug 2014

Role of relaxation time scale in noisy signal transduction

Alok Kumar Maity,[1,*] Pinaki Chaudhury,[1,†] and Suman K Banik[2,‡]

[1] *Department of Chemistry, University of Calcutta, 92 A P C Road, Kolkata 700 009, India*
[2] *Department of Chemistry, Bose Institute, 93/1 A P C Road, Kolkata 700 009, India*

(Dated: August 19, 2014)

Intracellular fluctuations, mainly triggered by gene expression, are an inevitable phenomenon observed in living cells. It influences generation of phenotypic diversity in genetically identical cells. Such variation of cellular components is beneficial in some contexts but detrimental in others. To quantify the fluctuations in a gene product, we undertake an analytical scheme for studying few naturally abundant linear as well as branched chain network motifs. We solve the Langevin equations associated with each motif under the purview of linear noise approximation and quantify Fano factor and mutual information. Both quantifiable expressions exclusively depend on the relaxation time (decay rate constant) and steady state population of the network components. We investigate the effect of relaxation time constraints on Fano factor and mutual information to indentify a time scale domain where a network can recognize the fluctuations associated with the input signal more reliably. We also show how input population affects both quantities. We extend our calculation to long chain linear motif and show that with increasing chain length, the Fano factor value increases but the mutual information processing capability decreases. In this type of motif, the intermediate components are shown to act as a noise filter that tune up input fluctuations and maintain optimum fluctuations in the output. For branched chain motifs, both quantities vary within a large scale due to their network architecture and facilitate survival of living system in diverse environmental conditions.

PACS numbers: 87.18.Mp, 05.40.-a, 87.18.Tt, 87.18.Vf

I. INTRODUCTION

Cell, building block of every biological system, is composed of some novel identical network motifs [1–5]. The ubiquitous examples of biological motifs are signal transduction network (STN) [6–10], gene transcription regulatory network (GTRN) [11–14], metabolic reaction network [15–17] as well as protein-protein interaction network [18, 19]. As cellular environment is stochastic in nature, it is interesting to investigate how these networks perform under fluctuating condition [20–26]. The extent of performance of a network is measured by the response time, i.e., how fast the network output is changed with the fluctuating input stimuli [27]. If the network input-output relation follows a characteristic time scale then it can sense the extra cellular changes more precisely via network components. Consequently, some intracellular changes are ensured with the variation of input signal with few chemical modifications to optimize the environmental effect. One of the well studied STNs is mitogen activated protein kinase (MAPK) cascade, mostly observed in eukaryotic signaling pathway [6–8]. In MAPK cascade, external signal is processed through several steps via phosphorelay mechanism and fluctuations in signaling molecules get modified at every step of the cascade. This phenomenon has been verified by using both experimental and theoretical studies in early literature, where the authors have shown that output fluctuations increase in an integrated way with cascade length [28–31]. In the case of GTRN, the network is depicted by few nodes that represent regulatory genes and are connected with few edges. A simplest motif can be constructed by considering two nodes representing two genes connected by a directed single edge. The edge signifies that product of one gene (transcription factor) regulates the other gene and the direction of the edge represents the mode of regulation. In such case, transcription factor may act as the signaling molecule and plays a pivotal role in maintaining the transcription rate of a target gene by controlling the appropriate time scale and the amount of transcriptional yield. GTRN motifs were initially identified in *E. coli* where few network motifs are much more common compared to the other random motifs [12, 32]. Later, these common motifs have been also observed in several other prokaryotes as well as in eukaryotes. To understand cellular physiology, it is very much essential to study GTRN motifs at the single cell level, because cell shows phenotypic heterogeneity in genetically identical system due to stochastic nature of these motifs. To this end, we have chosen few GTRN motifs to investigate the mode of functionality and their response under fluctuating environment.

In the present communication, we focus on few naturally abundant GTRN network motifs. At first, we consider a simple linear one step cascade (OSC) and study the steady state dynamical behavior under stochastic framework. Two nodes and one edge are used to draw this motif, where each node represents a gene of a simple regulatory system (see Fig. 1(a)). The edge indicates that one gene regulates the other via interaction of tran-

* alokkumarmaity@yahoo.co.in
† pinakc@rediffmail.com
‡ Corresponding author; skbanik@jcbose.ac.in

scription factor with the promoter site of the target gene. Due to the direct interaction of the two nodes, this motif can be considered as a direct pathway for gene regulation or signal transmission. The next motif we undertake is a linear two step cascade (TSC) obtained from the previous motif by inserting a new node (gene) in between the two nodes of the one step network (see Fig. 1(b)). In this case, the target gene is indirectly regulated by the input (transcription factors) that act as a signal.

Using the OSC and the TSC network motifs, we then construct some common motifs of biological importance that belong to a group, i.e., feed forward loop (FFL) (see Fig. 1(d-e)). We compose these motifs by lateral combination of two linear cascades (OSC and TSC). In FFL, a transcription factor regulates the target gene directly (via OSC) as well as indirectly (via TSC) [1, 2, 12, 32, 33]. In these motifs, two transcription factors are present and each of these can show either positive (activation) or negative (repression) effect on the target gene. Therefore, eight different types of FFL are possible considering both effects. Among all the possible FFL, four of these are of coherent type and the remaining four are of incoherent type. The classification is done according to the sign of the overall regulatory motif, positive and negative sign for coherent and incoherent type, respectively. Experimentally, it has been shown that type-1 FFL has both coherent and incoherent nature and are ubiquitous. Due to this reason, we consider these two motifs in the present work. Type-1 coherent FFL has two sub-types depending upon the function of direct and indirect regulatory pathways on the promoter region of the target gene. When both transcription factors are required to express the target gene, the FFL motif behaves as an AND like gate(see Fig. 1(e)). On the other hand, when one of the two transcription factors are sufficient to regulate the target gene, the FFL motif behaves as a OR like gate (see Fig. 1(d)). At this point, it is important to mention that few theoretical studies under stochastic framework have been undertaken to understand the FFL motif [22, 34–36].

We use a Gaussian model (see Models and Methods) to study the origin and consequence of stochasticity for all motifs considered in the present work. In all motifs, fluctuations are carried forward from one node to the next when signal is transduced along the direction of each edge. Thus, our main purpose here is the quantification of fluctuations in output signal for all motifs. Using an approximation technique (linear noise approximation), we solve all dynamical equations and calculate the Fano factor (variance/mean) [37] expression by which we measure output fluctuations of each motif. We also try to understand the effect of relaxation time scale, i.e., lifetime of a network component on output fluctuations as it can provide knowledge about each and every step of fluctuation propagation through a cascade. In other words, relaxation time scale of each network component provides a way to measure the amplification or suppression of fluctuations in each step of signal propagation.

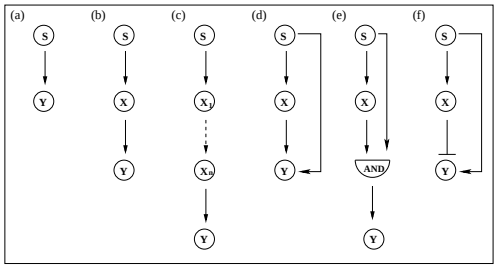

FIG. 1. Schematic presentation of different GTRN motifs (a) one step cascade (OSC), (b) two step cascade (TSC), (c) multi step cascade with n number of intermediate nodes, (d) OR coherent feed forward loop (OCFFL), (e) AND coherent feed forward loop (ACFFL) and (f) incoherent feed forward loop (ICFFL).

We derive a time scale condition in which fluctuations in the input signal are filtered out by the intermediate component. Similarly, conditions have been figured out when fluctuations are enhanced. We also examine the effect of copy numbers of input signal on output fluctuations and show that it plays a vital role under some specific conditions. As all cascades process information of the external signal, we investigate the reliability of information flow through each cascade by measuring the mutual information between the input signal and the output [38, 39]. We calculate the similar properties for FFL and identify different biological significance between two sub types of coherent motifs.

The rest of the paper is organized as follows. In the next section, we discuss about the generic model and methods employed in the present work. In Sec. III, results of individual motifs have been discussed. The paper is concluded in Sec. IV.

II. MODELS AND METHODS

To start with, we consider few network motifs that represent GTRN. All the motifs that are taken into account in the present work are shown in Fig. 1 where each circle represents a node and a straight line with an arrowhead connecting two different nodes represents an edge. The direction of an arrowhead denotes flow of signal from one node to the next one. The simplest linear signal transduction motif is modeled by two nodes, where S component acts as an input signal node (transcription factor) which regulates the expression of a target gene Y (Fig. 1(a)). The linear motif length is increased further by incorporating another node X in between the S and the Y nodes. In such a case, the S component regulates or transduces input signal to the Y component via the intermediate X (Fig. 1(b)) [4, 40, 41]. We also consider a long linear chain motif (Fig. 1(c)) by integrating n numbers of intermediate nodes within the simplest motif shown in Fig. 1(a).

Next, we focus on few branched chain network motifs that are constructed by lateral combination of the first two signal transduction motifs (one step and two step, Figs. 1(a-b)) in different ways and are characterized as feed forward loop (FFL). Fig. 1(d) represents coherent feed-forward loop of OR like gate (OCFFL), where the target gene Y is positively regulated by either the S or the X component, both acting as transcription factors. On the other hand, for coherent feed-forward loop of AND like gate (ACFFL), both S and X are essential to regulate the target gene Y positively (Fig. 1(e)). In Fig. 1(f), the transcription factor S positively regulates the production of gene Y in direct pathway but represses the gene regulation via the X mediated indirect pathway and this motif is known as incoherent feed-forward loop (ICFFL) [2, 32, 41].

All the biochemical network motifs considered in Fig. 1 consist of an input signal S and a output signal Y with an intermediate X except the long chain linear motif with n numbers of intermediate components (see Fig. 1(c)). We describe the time dependent dynamics of the three chemical components by a set of generic coupled Langevin equations which may be of linear or non linear type depending on the kinetic schemes of a network motif considered in the present work

$$\frac{ds}{dt} = f_s(s) - \tau_s^{-1} s + \xi_s(t), \tag{1}$$

$$\frac{dx}{dt} = f_x(s,x) - \tau_x^{-1} x + \xi_x(t), \tag{2}$$

$$\frac{dy}{dt} = f_y(s,x,y) - \tau_y^{-1} y + \xi_y(t). \tag{3}$$

In Eqs. (1-3), f_i and τ_i^{-1} represent the functional form of synthesis and degradation (inverse of life time τ_i) rate constants of the i-th ($i = s, x, y$) chemical component, respectively. Here, s, x and y stand for the chemical species S, X and Y, respectively. The noise terms ξ_i is considered to be Gaussian white noise with zero mean. The noise strength or the variance associated with each noise term can be written as $\langle|\xi_i|^2\rangle$, quantified by the sum of production and decay rate. The cross-correlation between two noise terms is zero as the two kinetics are uncorrelated with each other. Considering that the copy number of each component is large at steady state, we study the dynamics of each motif shown in Fig. 1, at steady state. Since the relaxation time of each component is small compared to the coarse grained (steady state) time scale, the Langevin equations we have adopted could satisfactorily explain the dynamics of each motif.

To solve the set of Langevin equations in a generalized way, we write these equations in the matrix form. To this end, we introduce two column vectors z and ξ where $z = (s, x, y)$ and $\xi = (\xi_s, \xi_x, \xi_y)$. Linearizing the Langevin equations around steady state and considering the change in copy number due to fluctuations of each species from steady state to be very small, one can write $\delta z(t) = z(t) - \langle z\rangle$, where $\langle z\rangle$ is the steady state value of z [42–46]. Performing Fourier transformation of the linearized equation, we obtain

$$i\omega\delta\tilde{z}(\omega) = J_{z=\langle z\rangle}\delta\tilde{z}(\omega) + \tilde{\xi}(\omega), \tag{4}$$

where $\tilde{z}(\omega)$ and $\tilde{\xi}(\omega)$ are Fourier transforms of $z(t)$ and $\xi(t)$, respectively. J is the Jacobian matrix evaluated at steady state. The diagonal elements of J define the relaxation time of each component and the off-diagonal terms take care of interaction between the two components. The power spectra of the network components can be derived using Eq. (4)

$$\mathcal{S}(\omega) = [i\omega I - J]^{-1} H \left[-i\omega I - J^T\right]^{-1}, \tag{5}$$

with I being the identity matrix. Elements of H stands for noise strength and J^T is the transpose of J. We perform the inverse Fourier transformation of power spectra for every network component at steady state and evaluate the variance as well as covariance of the individual component and between two components, respectively. From the variance of output component, one can quantify the extent of fluctuations that are transduced by the final transcript of all the network motifs considered and the quantity of fluctuations can be defined in terms of Fano factor $\sigma_y^2/\langle y\rangle$, ratio of variance and population of Y component [37]. We also calculate mutual information $\mathcal{I}(s,y)$ between the input signal and the output using Shannon formalism to check the reliability of all network motifs [38, 47, 48]

$$\mathcal{I}(s,y) = \frac{1}{2}\log_2\left[1 + \frac{\sigma_{sy}^4}{\sigma_s^2\sigma_y^2 - \sigma_{sy}^4}\right], \tag{6}$$

where σ_s^2 and σ_y^2 are the variance associated with the S and the Y component, respectively, and the covariance between them is given by σ_{sy}^2.

III. RESULTS AND DISCUSSIONS

In the following subsections, we execute individual study of each network motif as well as perform a comparative study of all the motifs. From the Fano factor expression, we can discriminate the origin of fluctuations of a motif. We identify the network that faces maximum fluctuating environment under a definite condition and characterize the favorable circumstances in which it can transduce the information of the input signal more reliably.

A. One step cascade

As one step cascade (OSC) is the simplest unit of addressing network motifs, we initially start with this simple motif. In this motif, the input signal S directly regulates the target gene Y. For the sake of simplicity, we consider that S is constitutively active and linearly regulates

TABLE I. Modified form of the analytical expression given by Eq. (9) for OSC motif. Fano factor ($\sigma_y^2/\langle y\rangle$) and co-variance ($\sigma_{sy}^2$) for different relaxation time limit are shown in this table.

	$\tau_s \gg \tau_y$	$\tau_s \approx \tau_y$	$\tau_s \ll \tau_y$
Fano factor	$1+\frac{\langle y\rangle}{\langle s\rangle}$	$1+0.5\frac{\langle y\rangle}{\langle s\rangle}$	$1+\frac{\tau_s\langle y\rangle}{\tau_y\langle s\rangle}$
σ_{sy}^2	$\langle y\rangle$	$0.5\langle y\rangle$	$\frac{\tau_s}{\tau_y}\langle y\rangle$

the target gene for the formation of Y. The stochastic reaction scheme in Langevin formalism is given by

$$\frac{ds}{dt} = k_1 - \tau_s^{-1}s + \xi_s(t), \tag{7}$$

$$\frac{dy}{dt} = k_3 s - \tau_y^{-1}y + \xi_y(t), \tag{8}$$

where k_1 and k_3 are the synthesis rate for S and Y, respectively. The degradation rates for the same components are given by τ_s^{-1} and τ_y^{-1}, respectively. $\xi_s(t)$ and $\xi_y(t)$ are Gaussian white noise terms with zero mean $\langle\xi_s(t)\rangle = \langle\xi_y(t)\rangle = 0$. The respective noise strengths are given by $\langle\xi_s(t)\xi_s(t')\rangle = 2\tau_s^{-1}\langle s\rangle\delta(t-t')$ and $\langle\xi_y(t)\xi_y(t')\rangle = 2\tau_y^{-1}\langle y\rangle\delta(t-t')$, respectively. In addition, both noise processes are uncorrelated, $\langle\xi_s(t)\xi_y(t')\rangle = \langle\xi_y(t)\xi_s(t')\rangle = 0$. We solve Eqs. (7-8) by the above mentioned procedure and calculate the variance associated with the output Y and co-variance between the input signal S and the output Y as [42–46]

$$\sigma_y^2 = \langle y\rangle + \frac{\tau_y^{-1}\langle y\rangle^2}{(\tau_s^{-1}+\tau_y^{-1})\langle s\rangle}, \sigma_{sy}^2 = \frac{\tau_y^{-1}\langle y\rangle}{\tau_s^{-1}+\tau_y^{-1}}. \tag{9}$$

In the above expression of variance σ_y^2, the first part on the right hand side arises due to intrinsic fluctuations in Y and the second part is responsible for extrinsic fluctuations, incorporated into the output Y through the input S during gene regulation. The total variance in this motif is expressed in terms of output variance σ_y^2 that follows spectral addition rule, sum of external and internal fluctuations [31, 49–53]. At this point, it is important to mention that two fluctuating terms originating from different sources have been also calculated for the oscillatory system [54]. In this study, we are interested in Fano factor as well as in information propagation through the cascade with the variation of system's relaxation times as well as steady state population $\langle s\rangle$ of the input component S, as both σ_y^2 and σ_{sy}^2 depend only on the time scale when the steady state value of both components $\langle s\rangle$ and $\langle y\rangle$ are kept fixed followed by a constant k_1/τ_s^{-1} and k_3/τ_y^{-1} ratio. Similarly, for constant relaxation times, both expressions vary with the steady state populations $\langle s\rangle$ and $\langle y\rangle$. In this motif, we have two relaxation time scales τ_s (input) and τ_y (output). These two time scales lead to three possible limiting conditions for which we get three different modified expressions for Fano factor ($\sigma_y^2/\langle y\rangle$) as well as for co-variance (see Table I).

In Table I, Fano factor and σ_{sy}^2 values are maximum at the time limit $\tau_s \gg \tau_y$ whereas, both are minimum at the time limit $\tau_s \ll \tau_y$. These results reveal that the effect of input fluctuations into the output fluctuations gets maximized if the input signal relaxes at a much slower rate compared to the output signal ($\tau_s^{-1} \ll \tau_y^{-1}$) and will be minimized for faster input relaxation rate compared to the output one ($\tau_s^{-1} \gg \tau_y^{-1}$). However, the output signal faces an intermediate level of fluctuations when both signals have comparable relaxation rate ($\tau_s^{-1} \approx \tau_y^{-1}$).

For faster fluctuations in the input component ($\tau_s \ll \tau_y$), the target gene cannot sense the rapid concentration changes of the input signal and shows an average response. In such a case, external fluctuations have no significant contribution in the fluctuations of output and consequently, suppression of the output fluctuations is executed and minimum Fano factor value is obtained. In this connection, it is important to mention that for very large τ_y, the ratio τ_s/τ_y is very low ($\ll 1$) and contribution of extrinsic fluctuations becomes insignificant in the total output fluctuations. Therefore, output fluctuations only depend on the mean steady state value of the target gene and the network motif follows a Poisson statistic, i.e., behaves like a simple birth-death process (Fano factor $\sigma_y^2/\langle y\rangle = 1$). However, the target gene successfully characterizes the concentration change of signaling molecule for slower input fluctuations ($\tau_s \gg \tau_y$). In this time scale, the OSC motif transduces extracellular or upstream signal reliably and provides an exact response with the achievement of maximum Fano factor. When both time scales are approximately equal ($\tau_s \approx \tau_y$), extrinsic fluctuations get partially incorporated into the total fluctuations and give an intermediate Fano factor value which is in between the two extreme cases, slowest and fastest input fluctuations. It seems apparent that the motif can sense external fluctuations with a greater extent in the nearly equal relaxation time scales but our result does not show that. As both reactions are stochastic in nature, they have probabilistic character that executes two chance factors. In one situation, the target gene can properly characterize the input fluctuations and in the other situation, it fails to characterize the same. This results into a statistical weightage value of 0.5 in the contribution of extrinsic fluctuations in the Fano factor expression. A similar kind of time scale effect is also shown by the co-variance expression which governs the mutual information transduction. In Figs. 2(a-b), we show surface plots of Fano factor and mutual information, respectively, as a function of two relaxation rate constants, τ_y^{-1} and τ_s^{-1}, where we maintain the steady state population of both components by a constant parameters ratio $k_1/\tau_s^{-1} = k_3/\tau_3^{-1} = 10$. Fig. 2(a) shows that the maximum Fano factor value is attained by the motif only at very low input relaxation rate constant compared to the output one. Along diagonal axis both rate constants are approximately equal. Hence, the magnitude of Fano factor is within an intermediate range. The minimum level of Fano factor value is observed at very high input rate constant compared to the output one. In Fig. 2(b), the 2d-plot of mutual information also

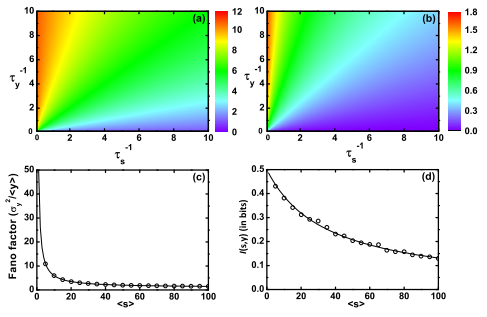

FIG. 2. (Color online) The OSC. (a, b) Two dimensional maps of Fano factor and mutual information $\mathcal{I}(s, y)$, respectively, as a function of two relaxation rate constants τ_y^{-1} and τ_s^{-1} for the ratio $k_1/\tau_s^{-1} = k_3/\tau_y^{-1} = 10$. (c) Fano factor and (d) mutual information $\mathcal{I}(s, y)$ profiles as a function of mean input signal level $\langle s \rangle$. Parameters used are $\tau_s^{-1} = \tau_y^{-1} = 1.0$ and $k_3 = 100/k_1$. The symbols are generated using stochastic simulation algorithm [55, 56] and the lines are due to theoretical calculation.

varies in a similar fashion as the Fano factor plot. As the OSC motif performs under the definite input fluctuations, the information transduction capability of the motif is mainly characterized on the basis of input-output relaxation time scales. As a result, the motif can transude the input information more reliably at faster relaxation time scale of the output component among all the relaxation time scales of output component (see the three limiting conditions in Table I).

For the three relaxation time limiting cases given in Table I, the Fano factor expression also depends on the steady state population of the network components. However, from the Fano factor expression it is clear that extrinsic fluctuations can contribute an appreciable amount in the total output noise if the steady state population of output component is much higher than the input one. This means that for a highly populated input signal, the fluctuations in the input do not have significant effect on the regulation of the target gene. Consequently, the regulated gene works under an apparently constant level of the input signal. Therefore, the motif shows low level of Fano factor value even if it belongs to the relaxation time scale limit where maximum input fluctuations are transduced. In Fig. 2(c), we show the Fano factor associated with the variation of population of the signaling molecule S. In this plot, a sharp exponential decay of the Fano factor is observed as the steady state population of the input signal increases. In Fig. 2(d), mutual information $\mathcal{I}(s, y)$ is plotted as a function of the input signal. In Figs. 2(c-d), population level of the input signal is systematically increased by increasing the synthesis rate constant k_1 whereas, the steady state population of the output Y is kept fixed by simultaneous change of the synthesis rate constant k_3, followed by a mathematical relation $k_3 = 100/k_1$. The rest of the parameter values used are $\tau_1^{-1} = \tau_3^{-1} = 1.0$. In the mutual information plot (Fig. 2(d)), sharp exponential decay is not observed as in Fig. 2(c). This happens due to the absence of explicit dependence of signaling molecule in the expression of co-variance (see Eq. (9)) and for keeping $\langle y \rangle$ fixed. In addition, in the expression of mutual information (see Eq. (6)), the input signal has a predominant effect due to σ_s^2 that overcomes the decreasing effect of σ_y^2 associated with Y.

Based on the analysis provided in the aforesaid discussion, one can compare the OSC motif with the well known motif of gene transcription and translation machinery. Here, mRNA, the product of transcription can be considered as signaling component S generated from a fully induced or a constitutive promoter at a constant rate. Similarly, protein, the product of translation plays the role of component Y translated from mRNA. If one does not take into account the genetic switching steps (on/off state of a promoter) then one can easily compare the gene regulation network with the OSC motif where mRNA (S) and protein (Y) represent the input and the output component, respectively. From the conditions presented in Table I, one can conclude that the gene regulation motif can only attain a low level of fluctuations in the protein level through high population and relaxation rate constant of the input component compared to the output one. Thus, fluctuations in the protein Y, the gene product, are modulated via kinetic parameter as well as deterministic population of mRNA which acts as signaling component S. Protein molecule shows minimum fluctuations under the constraints of large number of mRNA with very low average lifetime τ_s. These phenomena have been verified extensively via experimental and theoretical studies [20, 49, 51, 57–63]. Similarly, an extensive study on noise propagation in eukaryotic gene expression has been accomplished using data from two high-throughput experiments where Fraser et al [60] have observed that the production of essential and complex-forming proteins implicate low level of fluctuations compared to other proteins and this low level of fluctuations is attained via high transcription rate and low translation efficiency. Due to a high transcription rate, a large amount of mRNA is generated. While doing the analysis, they have used the definition of the translation efficiency, ratio of protein synthesis and mRNA decay rate constant. Translation efficiency can be minimized for very high decay (relaxation) rate constant of mRNA molecule, i.e., very short lifetime under a constant protein production rate. From our calculation, we also get an equivalent result that successfully explicates their noble findings.

B. Two step cascade

In two step cascade (TSC)(see Fig. 1(b)), the output component Y is indirectly regulated by the input component S via an intermediate component X. As the dynamical equation for the input signal S is same as in

the previous motif (Eq. (7)), we do not write it here explicitly. The Langevin equations for the remaining two components X and Y are given as

$$\frac{dx}{dt} = k_2 s - \tau_x^{-1} x + \xi_x(t), \tag{10}$$

$$\frac{dy}{dt} = k_3 x - \tau_y^{-1} y + \xi_y(t). \tag{11}$$

In the above equations, k_2 and k_3 are the synthesis rate constants of X and Y component, respectively. τ_i^{-1} and $\xi_i(t)$ $(i = x, y)$ are decay rate constants and Langevin force terms of the respective component. As in the OSC, the three noise terms (ξ_s, ξ_x and ξ_y) here are Gaussian white type with similar noise properties. Solving the Langevin equations in a similar manner [42–46], we get the expression of variance and co-variance of the output component Y

$$\sigma_y^2 = \langle y\rangle + \frac{\tau_y^{-1}\langle y\rangle^2}{(\tau_x^{-1}+\tau_y^{-1})\langle x\rangle} + \frac{\tau_x^{-1}\tau_y^{-1}(\tau_s^{-1}+\tau_x^{-1}+\tau_y^{-1})\langle y\rangle^2}{(\tau_s^{-1}+\tau_x^{-1})(\tau_x^{-1}+\tau_y^{-1})(\tau_s^{-1}+\tau_y^{-1})\langle s\rangle},$$

$$\sigma_{sy}^2 = \frac{\tau_x^{-1}\tau_y^{-1}\langle y\rangle}{(\tau_s^{-1}+\tau_x^{-1})(\tau_s^{-1}+\tau_y^{-1})}. \tag{12}$$

The first term on the right hand side of the variance σ_y^2 reveals the intrinsic fluctuations in the output component Y. The second and the third terms of the expression originate due to the fluctuations in the X and the S component, respectively. Compared to the OSC motif, an extra noise term appears in the variance which originates due to the addition of intermediate component X. Hence, the magnitude of total output fluctuations in TSC becomes higher compared to the OSC. If one inserts a new intermediate component into the TSC motif, the output fluctuations will increase further. This indicates that the output fluctuations are increased with the augmentation of cascade length. Such fluctuations integration character in each step of a cascade has been verified earlier both experimentally and theoretically [28–31]. In spite of these fluctuations enhancement property of long chain cascade networks, some long chain network motifs like MAPK signaling pathways as well as GTRNs are identified in living systems, where external signal gets transduced with great accuracy. This is an unusual but interesting aspect of living beings that promotes an extra curiosity to study signaling pathways to understand the execution of high precision signal transduction in highly fluctuating environment. While considering the dynamics of TSC, we try to decipher the criteria that leads to the understanding of the formation of final output Y under the condition of optimum fluctuations as per the system's permissibility. In Eq. (12), both expressions depend on the three relaxation rate constants τ_s^{-1}, τ_x^{-1} and τ_y^{-1} as well as on the steady state population level of the network components ($\langle s\rangle$, $\langle x\rangle$ and $\langle y\rangle$). Possible combinations of three relaxation times (τ_s, τ_x and τ_y) leads to nine different modified

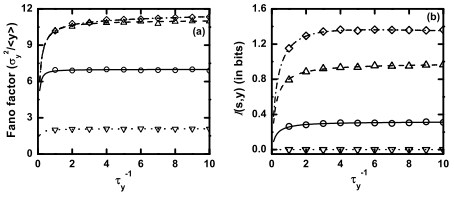

FIG. 3. The TSC. (a) Fano factor and (b) mutual information $\mathcal{I}(s, y)$ profiles as a function of relaxation rate constant τ_y^{-1} of Y component. $k_1/\tau_s^{-1} = k_2/\tau_x^{-1} = 10$ and $k_3/\tau_y^{-1} = 1.0$ are maintained throughout these plots, so that steady state population of all the components remains unaltered. In both plots, for solid (with open circles), dashed (with open upward triangle), dotted (with open downward triangle) and dash dotted (with open diamond) lines we have used the relations $\tau_s^{-1} = \tau_x^{-1} = 0.1$, $\tau_s^{-1} = \tau_x^{-1}/10 = 0.1$, $\tau_s^{-1}/100 = \tau_x^{-1} = 0.1$ and $\tau_s^{-1} = \tau_x^{-1}/100 = 0.1$, respectively. The symbols are generated using stochastic simulation algorithm [55, 56] and the lines are due to theoretical calculation.

expressions of Fano factor ($\sigma_y^2/\langle y\rangle$) and co-variance ($\sigma_{sy}^2$), shown in Table II.

From the modified expressions given in Table II it is easy to identify the maximum, intermediate and minimum value of Fano factor and co-variance under the condition $\tau_s \gg \tau_x \gg \tau_y$, $\tau_s \approx \tau_x \approx \tau_y$ and $\tau_s \ll \tau_x \ll \tau_y$, respectively. In all the expressions, effect of the population level of the input and the intermediate component on the output is clearly visible. As our main focus in the present study is to characterize the effect of relaxation time scales in terms of Fano factor and co-variance, we fix the steady state population of all the network components using the relations $k_1/\tau_s^{-1} = k_2/\tau_x^{-1} = 10$ and $k_3/\tau_y^{-1} = 1.0$. In Figs. 3, we show Fano factor and mutual information for the TSC motif as a function of output relaxation rate constant τ_y^{-1} for different values of τ_s^{-1} and τ_x^{-1}.

From the plot shown in Fig. 3(a), it is clear that Fano factor value increases with the increment of output relaxation rate constant τ_y^{-1} for all sets of parameter values. As the output component Y can track the comparably slower fluctuations of upstream input signal efficiently, fluctuations of the output component increases proportionately with its relaxation rate constant. The additive nature of fluctuations assists to amplify the Fano Factor value through total output as a function of τ_y^{-1} and the trend is persistent for all the four sets of parameter values used to draw Fig. 3(a). Among the four sets of parameters, higher Fano factor values are achieved by two sets of parameters. From the parameter sets $\tau_s^{-1} = \tau_x^{-1}/10 = 0.1$ and $\tau_s^{-1} = \tau_x^{-1}/100 = 0.1$, it is evident that the intermediate component X has faster fluctuations rate than the input component S ($\tau_x^{-1} \gg \tau_s^{-1}$). As a result, it becomes possible for X to characterize the fluctuations in S. At the equal relaxation time scale limits of S and X ($\tau_s^{-1} = \tau_x^{-1} = 0.1$), we get an intermediate Fano factor profile and a minimum profile of the same is

TABLE II. Modified forms of the analytical solution (Eq. (12)) of TSC motif. Fano factor ($\sigma_y^2/\langle y\rangle$) and co-variance ($\sigma_{sy}^2$) at different relaxation time limits are shown with $\rho = \tau_s/(\tau_s+\tau_y) \leqslant 1$.

		$\tau_x \gg \tau_y$	$\tau_x \approx \tau_y$	$\tau_x \ll \tau_y$
$\tau_s \gg \tau_x$	Fano factor	$1+\frac{\langle y\rangle}{\langle x\rangle}+\frac{\langle y\rangle}{\langle s\rangle}$	$1+0.5\frac{\langle y\rangle}{\langle x\rangle}+\frac{\langle y\rangle}{\langle s\rangle}$	$1+\frac{\tau_x\langle y\rangle}{\tau_y\langle x\rangle}+\rho\frac{\langle y\rangle}{\langle s\rangle}$
	σ_{sy}^2	$\langle y\rangle$	$\langle y\rangle$	$\rho\langle y\rangle$
$\tau_s \approx \tau_x$	Fano factor	$1+\frac{\langle y\rangle}{\langle x\rangle}+0.5\frac{\langle y\rangle}{\langle s\rangle}$	$1+0.5\frac{\langle y\rangle}{\langle x\rangle}+\frac{3\langle y\rangle}{8\langle s\rangle}$	$1+\frac{\tau_x\langle y\rangle}{\tau_y\langle x\rangle}+\frac{\tau_x\langle y\rangle}{\tau_y\langle s\rangle}$
	σ_{sy}^2	$0.5\langle y\rangle$	$0.25\langle y\rangle$	$0.5\frac{\tau_s\langle y\rangle}{\tau_y}$
$\tau_s \ll \tau_x$	Fano factor	$1+\frac{\langle y\rangle}{\langle x\rangle}+\frac{\tau_s\langle y\rangle}{\tau_x\langle s\rangle}$	$1+0.5\frac{\langle y\rangle}{\langle x\rangle}+0.5\frac{\tau_s\langle y\rangle}{\tau_x\langle s\rangle}$	$1+\frac{\tau_x\langle y\rangle}{\tau_y\langle x\rangle}+\frac{\tau_s\langle y\rangle}{\tau_y\langle s\rangle}$
	σ_{sy}^2	$\frac{\tau_s\rho\langle y\rangle}{\tau_x}$	$\frac{\tau_s^2\langle y\rangle}{\tau_x\tau_y}$	$\frac{\tau_s^2\langle y\rangle}{\tau_x\tau_y}$

obtained for $\tau_s^{-1}/100 = \tau_x^{-1} = 0.1$. This happens as the S component fluctuates in a faster time scale compared to the X component which, in turn, forbids X to differentiate the concentration change in S. As a result, X is unable to carry forward the variation in signal due to S to the Y component of the TSC motif. In this relaxation time scale limit, the intermediate X acts as a low pass filter that passes only low-frequency input signal. For this reason, highly fluctuating (high-frequency) input signal is impeded by the intermediate component that inhibits fluctuations propagation through the motif.

In Fig. 3(b), mutual information $\mathcal{I}(s,y)$ flow varies with the relaxation rate of Y and we observe that TSC motif transduces information more reliably at faster fluctuations in Y due to proper characterization of the input signal variation and is applicable for different choice of parameters sets. For the four sets of parameters, mutual information follows the increasing trend of Fano factor but, it is important to mention that for $\tau_s^{-1}/100 = \tau_x^{-1} = 0.1$, $\mathcal{I}(s,y)$ value is almost zero. This happens due to slow fluctuations in X compared to S which impedes the flow of information due to input signal into the downstream component. As a result, the intermediate component cannot discriminate the variation of external signal and gives a constant response to the change in the environment. Although the Fano factor is minimum at this time frame, the TSC motif is unable to adapt due to the approximately zero mutual information processing ability. Hence, the network motif opts for a relaxation time scale where both fluctuations and mutual information processing capacity adopts an optimum value.

Next, we extend our calculation for a generalized motif of linear long chain cascade (see Fig. 1(c)) considering n numbers of different intermediate components (X_1, X_2, .., X_n) that are present in between the input and the output component. Using the concept of TSC motif, we obtain the expressions of Fano factor for three limiting relaxation rate conditions as

$$1+\frac{\langle y\rangle}{\langle x_n\rangle}+\cdots+\frac{\langle y\rangle}{\langle x_1\rangle}+\frac{\langle y\rangle}{\langle s\rangle}$$
$$\text{for } \tau_y \gg \tau_{x_n} \gg \cdots \gg \tau_{x_1} \gg \tau_s,$$
$$1+c_n\frac{\langle y\rangle}{\langle x_n\rangle}+\cdots+c_1\frac{\langle y\rangle}{\langle x_1\rangle}+c_s\frac{\langle y\rangle}{\langle s\rangle}$$
$$\text{for } \tau_y \approx \tau_{x_n} \approx \cdots \approx \tau_{x_1} \approx \tau_s,$$
$$1+\frac{\tau_{x_n}\langle y\rangle}{\tau_y\langle x_n\rangle}+\cdots+\frac{\tau_{x_1}\langle y\rangle}{\tau_y\langle x_1\rangle}+\frac{\tau_s\langle y\rangle}{\tau_y\langle s\rangle}$$
$$\text{for } \tau_y \ll \tau_{x_n} \ll \cdots \ll \tau_{x_1} \ll \tau_s.$$

where $c_1,\cdots,c_n \leqslant 0.5$, $c_s \leqslant 0.5$ and $\tau_{x_1},\tau_{x_2},\cdots,\tau_{x_n}$ are the relaxation time of the X_1, X_2, $\cdots$, X_n component, respectively. The expressions given above are three simplified forms of Fano factor expressions for linear long chain signal transduction motif or GTRN cascade with n number of different intermediate components. The main motivation to evaluate these simplified forms is that using the expressions, one can easily get a gross quantitative idea about the output fluctuations of any linear chain network cascade with large number of intermediate components. If one knows the steady state population level of the network components as well as lifetime of the same then only using those parameters one can calculate Fano factor quantity that will provide a hint about the networks fluctuations. This is the main advantage of the present formalism that makes easier the study of stochastic features of several unexplored systems.

In the aforesaid discussion, we have searched for the effect of relaxation time scale on signal transduction machinery through linear type of GTRN motifs. These results suggest us to extend our analysis to motifs having branched pathway. The branched pathway motifs are generated with the help of lateral combinations of more than one linear pathway motifs. Therefore, our next objective is to investigate the relaxation time scale effect on a family of branched network such as feed forward loop (FFL) [2, 12, 32, 33]. FFL appears more frequently in gene networks of *E. coli*, *S. cerevisiae* and other living organisms. It consists of three genes which are characterized by three different transcription factors S, X and Y where X regulates Y and S regulates both X and Y. Thus, S directly as well as indirectly, via X, regulates Y

leading to positive (activation) or negative (repression) transcription interaction. Sign of the direct regulation path is equal to the indirect path for coherent feed forward loop (CFFL) but opposite sign of two regulatory pathways is the basis for incoherent feed forward loop (ICFFL). Although eight FFL are possible from structural configuration, we study only two most abundant network motifs, type-1 CFFL and ICFFL. The FFL networks have two input signals, one signal induces the S encoded transcription factor gene and the other induces the X encoded gene. For the sake of simplicity, we investigate these motifs under the effect of constant input signal. In the following subsections, we discuss the role of different time scales on the two FFL motifs.

C. Coherent feed forward loop

In type-1 CFFL motif, both S and X either positively or negatively regulate the promoter of the target gene Y. The expression level of output Y is controlled by the concentration of two upstream transcription factors. If both S and X are required to control the production of Y, the motif behaves as AND like logic gate otherwise it behaves as an OR like logic gate. Keeping this in mind, we examine these two architectures and investigate which one of these two faces maximum fluctuations in a noisy environment.

1. OR like gate

In OR like CFFL (OCFFL) motif (Fig. 1(d)), any one of the two upstream components (S and X) is sufficient to control the expression of Y. Hence, in the dynamical equation of Y, we introduce two different synthesis rate constants, k_3' and k_3 for the direct and the indirect regulation pathways, respectively. These two rate constants give freedom to tune up the extent of interaction amid the transcription factor and the target gene in an independent way. The first term defines the extent of interaction to express Y via direct pathway and the second one is responsible for the indirect pathway. From the logical condition, either of the two interactions of this motif is predominant over the other, i.e., if the direct regulation is stronger then the indirect regulation must be weaker, or vice versa. When the direct regulation path is more prominent, the motif behaves like the OSC but if the indirect path plays a pivotal role, then it performs as the TSC. Keeping this in mind, we write the stochastic dynamical equations as

$$\frac{dx}{dt} = k_2 s - \tau_x^{-1} x + \xi_x(t), \tag{13}$$

$$\frac{dy}{dt} = k_3' s + k_3 x - \tau_y^{-1} y + \xi_y(t). \tag{14}$$

While writing the above equations, we do not explicitly show the dynamical equation for S component but use the previously written Eq. (7) for the OSC. Using usual method of solution, we evaluate the following expression of variance and co-variance

$$\sigma_y^2 = \langle y\rangle + \frac{\tau_y^{-1}\beta^2\langle x\rangle}{(\tau_x^{-1}+\tau_y^{-1})} + \frac{\tau_y^{-1}\gamma^2\langle s\rangle}{(\tau_s^{-1}+\tau_y^{-1})} + p\frac{\tau_x^{-1}\tau_y^{-1}(\tau_s^{-1}+\tau_x^{-1}+\tau_y^{-1})\langle s\rangle}{(\tau_s^{-1}+\tau_x^{-1})(\tau_x^{-1}+\tau_y^{-1})(\tau_s^{-1}+\tau_y^{-1})},$$

$$\sigma_{sy}^2 = \frac{\tau_y^{-1}\langle y\rangle}{(\tau_s^{-1}+\tau_y^{-1})} - \frac{\tau_s^{-1}\tau_y^{-1}\beta\langle x\rangle}{(\tau_s^{-1}+\tau_x^{-1})(\tau_s^{-1}+\tau_y^{-1})}, \tag{15}$$

where α, β, γ and p are $k_2/\tau_x^{-1}, k_3/\tau_y^{-1}$, k_3'/τ_y^{-1} and $\alpha^2\beta^2 + 2\alpha\beta\gamma$, respectively. All the rate constants define their usual meaning in the above kinetic equations (Eqs. (13-14)). To understand the effect of relaxation time scale on this model, we take all possible relations among the three relaxation time constants and obtain nine conditions using which modified expressions of Fano factor and co-variance are calculated (see Table III).

Similar to our previously discussed motifs, the OCFFL motif also accomplishes maximum, intermediate and minimum values of Fano factor and co-variance for the three separate relaxation time limiting conditions $\tau_s \gg \tau_x \gg \tau_y$, $\tau_s \approx \tau_x \approx \tau_y$ and $\tau_s \ll \tau_x \ll \tau_y$. These modified (maximum, intermediate and minimum) forms are given in Table III. For OCFFL, we do not explore graphically the role of relaxation rate constant τ_y^{-1} on Fano factor and mutual information. Due to the presence of an interesting feature in this motif by the virtue of direct and indirect contribution of two regulatory pathways in gene regulation via S and X, respectively, we look at the dependence of the rate constants k_3' and k_3. Since, on the basis of the dominating power amid the two rate constants, the OCFFL motif can reduce to either OSC or TSC, we investigate the effect of these synthesis rate constants on the fluctuations and mutual information propagation. We show Fano factor and mutual information $\mathcal{I}(s,y)$ as a function of k_3' in Fig. (4). For both plots, we maintain a constant pool of the steady state population level of the Y component using the relation $(10k_3 + k_3')/\tau_y^{-1} = 10$ and set a high value of the relaxation rate constant $\tau_y^{-1} = 10$. Only in this relaxation time domain, the output component can track fluctuations in the upstream signal very accurately.

In Fig. (4), we increase the influence of direct regulatory pathway with the help of augmentation of the S dependent synthesis rate constant k_3' of the Y component. By doing this, we increase the contribution of the OSC motif in the OCFFL but decrease the contribution of X dependent synthesis rate constant k_3 due to the relation $(10k_3 + k_3')/\tau_y^{-1} = 10$. In Fig. 4(a), Fano factor profile slowly goes down with k_3' for $\tau_s^{-1} = \tau_x^{-1}/10 = 0.1$ and $\tau_s^{-1} = \tau_x^{-1}/100 = 0.1$. At these two limits, fluctuations can propagate through this motif very smoothly. For very low value of k_3', the OCFFL motif behaves as a TSC with high Fano factor value. On the other hand, for high value of k_3', the OCFFL motif behaves as a

TABLE III. Modified forms of the analytical solution (Eq. (15)) of OCFFL motif. Fano factor ($\sigma_y^2/\langle y\rangle$) and co-variance ($\sigma_{sy}^2$) at different relaxation time limits are shown where $\rho = \tau_s/(\tau_s+\tau_y) \leqslant 1$, $\alpha = k_2/\tau_x^{-1}$, $\beta = k_3/\tau_y^{-1}$, $\gamma = k_3'/\tau_y^{-1}$ and $p = \alpha^2\beta^2 + 2\alpha\beta\gamma$.

		$\tau_x \gg \tau_y$	$\tau_x \approx \tau_y$	$\tau_x \ll \tau_y$
$\tau_s \gg \tau_x$	Fano factor	$1+\frac{\beta^2\langle x\rangle}{\langle y\rangle}+\frac{(\gamma^2+p)\langle s\rangle}{\langle y\rangle}$	$1+0.5\frac{\beta^2\langle x\rangle}{\langle y\rangle}+\frac{(\gamma^2+p)\langle s\rangle}{\langle y\rangle}$	$1+\frac{\beta^2\tau_x\langle x\rangle}{\tau_y\langle y\rangle}+\rho\frac{(\gamma^2+p)\langle s\rangle}{\langle y\rangle}$
	σ_{sy}^2	$\langle y\rangle - \frac{\tau_x\beta\langle x\rangle}{\tau_s}$	$\langle y\rangle - \frac{\tau_x\beta\langle x\rangle}{\tau_s}$	$\rho(\langle y\rangle - \frac{\tau_x\beta\langle x\rangle}{\tau_s})$
$\tau_s \approx \tau_x$	Fano factor	$1+\frac{\beta^2\langle x\rangle}{\langle y\rangle}+\frac{(\gamma^2+0.5p)\langle s\rangle}{\langle y\rangle}$	$1+0.5\frac{\beta^2\langle x\rangle}{\langle y\rangle}+\frac{(0.5\gamma^2+\frac{3p}{8})\langle s\rangle}{\langle y\rangle}$	$1+\frac{\beta^2\tau_x\langle x\rangle}{\tau_y\langle y\rangle}+\frac{\tau_s(\gamma^2+p)\langle s\rangle}{\tau_y\langle y\rangle}$
	σ_{sy}^2	$\langle y\rangle - 0.5\beta\langle x\rangle$	$0.5\langle y\rangle - 0.25\beta\langle x\rangle$	$\frac{\tau_s(\langle y\rangle - 0.5\beta\langle x\rangle)}{\tau_y}$
$\tau_s \ll \tau_x$	Fano factor	$1+\frac{\beta^2\langle x\rangle}{\langle y\rangle}+\frac{(\rho\gamma^2+\frac{\tau_s p}{\tau_x})\langle s\rangle}{\langle y\rangle}$	$1+0.5\frac{\beta^2\langle x\rangle}{\langle y\rangle}+\frac{\tau_s(\gamma^2+0.5p)\langle s\rangle}{\tau_y\langle y\rangle}$	$1+\frac{\beta^2\tau_x\langle x\rangle}{\tau_y\langle y\rangle}+\frac{\tau_s(\gamma^2+p)\langle s\rangle}{\tau_y\langle y\rangle}$
	σ_{sy}^2	$\rho(\langle y\rangle - \beta\langle x\rangle)$	$\frac{\tau_s(\langle y\rangle - \beta\langle x\rangle)}{\tau_y}$	$\frac{\tau_s(\langle y\rangle - \beta\langle x\rangle)}{\tau_y}$

OSC with comparatively low Fano factor value. For the rest of the two parameter sets ($\tau_s^{-1} = \tau_x^{-1} = 0.1$ and $\tau_s^{-1}/100 = \tau_x^{-1} = 0.1$), the Fano factor value increases with k_3' as fluctuations propagation is hindered by the intermediate component X due to the indirect pathway. At these limits, for low value of k_3', the motif attains a lower Fano factor value but as the value of k_3' increases, the extent of OSC character plays a dominant role which in turn increases the Fano factor value and fluctuations propagation becomes smooth via the direct pathway without any sort of intermediate obstacle.

In Fig. 4(b), we show the mutual information $\mathcal{I}(s,y)$ in between the input signal S and the output Y as a function of k_3'. The profile shows an increasing trend and is valid for all sets of parameter considered. Information processing is mainly affected by fluctuations and number of intermediate component(s) in between the input and the output of the corresponding network. Hence, at low value of k_3', lesser amount of signal is transmitted compared to high value of k_3' due to the transition from effective TSC character to effective OSC character as k_3' is increased.

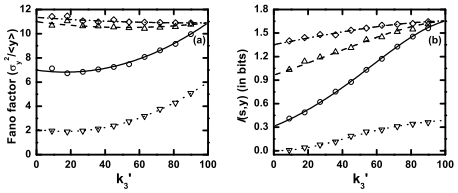

FIG. 4. The OCFFL. (a) Fano factor and (b) mutual information $\mathcal{I}(s,y)$ profiles as a function of S dependent synthesis rate constant $k_3^{'}$ of Y component. The relations $k_1/\tau_s^{-1} = k_2/\tau_x^{-1} = 10$, $(10k_3 + k_3^{'})/\tau_y^{-1} = 10$ and τ_y^{-1}=10 are maintained so that steady state population of all the components remain unaltered. In both plots, for solid (with open circles), dashed (with open upward triangle), dotted (with open downward triangle) and dash dotted (with open diamond) lines we have used $\tau_s^{-1} = \tau_x^{-1} = 0.1$, $\tau_s^{-1} = \tau_x^{-1}/10 = 0.1$, $\tau_s^{-1}/100 = \tau_x^{-1} = 0.1$ and $\tau_s^{-1} = \tau_x^{-1}/100 = 0.1$, respectively. The symbols are generated using stochastic simulation algorithm [55, 56] and the lines are due to theoretical calculation.

Among the four parameter sets considered, exceptionally low $\mathcal{I}(s,y)$ value is obtained for $\tau_s^{-1}/100 = \tau_x^{-1} = 0.1$ due to faster fluctuations rate of S component than X and Y components. Living systems having the OCFFL motif have a great advantage of adopting either of the two linear cascades (OSC or TSC) with the variation of weightage on direct or indirect pathway of gene regulation. Thus, any system when gives an extra importance on the TSC, attains maximum output fluctuations with minimum mutual information but attains reverse results by giving importance to the OSC motif. A trade off between output fluctuations and mutual information may be accomplished by the system using these two pathways, direct and indirect. Therefore, the essence of this motif is that during evolution it has been designed in a way that makes a living system more adaptable within any diverse environmental situation.

2. *AND like gate*

In the AND like CFFL (ACFFL) motif (Fig. 1(e)), both S and X jointly regulate the target gene Y. Thus, in the dynamical equation of Y, the synthesis term is expressed in terms of both S and X. Other than this synthesis part, rest of the equations of all the dynamical components are the same as the OCFFL motif,

$$\frac{dx}{dt} = k_2 s - \tau_x^{-1}x + \xi_x(t), \tag{16}$$

$$\frac{dy}{dt} = k_3 sx - \tau_y^{-1}y + \xi_y(t). \tag{17}$$

In the above set of equations, all the rate constants define kinetic significance of the corresponding network components. Here, we also do not rewrite the dynamical equation for S and use the previous equation (Eq. (7)). We solve the set of dynamical equations considering an approximation $\langle sx\rangle = \langle s\rangle\langle x\rangle$ [42–46] as reactions in between the two components S and X are uncorrelated with each other and obtain simplified analytical form of variance

TABLE IV. Modified forms of the analytical solution (Eq. 18) of ACFFL motif. Fano factor ($\sigma_y^2/\langle y\rangle$) and co-variance ($\sigma_{sy}^2$) at different relaxation time limits are shown where $\rho = \tau_s/(\tau_s+\tau_y) \leqslant 1$.

		$\tau_x \gg \tau_y$	$\tau_x \approx \tau_y$	$\tau_x \ll \tau_y$
$\tau_s \gg \tau_x$	Fano factor	$1+\frac{\langle y\rangle}{\langle x\rangle}+4\frac{\langle y\rangle}{\langle s\rangle}$	$1+0.5\frac{\langle y\rangle}{\langle x\rangle}+4\frac{\langle y\rangle}{\langle s\rangle}$	$1+\frac{\tau_x\langle y\rangle}{\tau_y\langle x\rangle}+4\rho\frac{\langle y\rangle}{\langle s\rangle}$
	σ_{sy}^2	$2\langle y\rangle$	$2\langle y\rangle$	$2\rho\langle y\rangle$
$\tau_s \approx \tau_x$	Fano factor	$1+\frac{\langle y\rangle}{\langle x\rangle}+2.5\frac{\langle y\rangle}{\langle s\rangle}$	$1+0.5\frac{\langle y\rangle}{\langle x\rangle}+\frac{13\langle y\rangle}{8\langle s\rangle}$	$1+\frac{\tau_x\langle y\rangle}{\tau_y\langle x\rangle}+4\frac{\tau_x\langle y\rangle}{\tau_y\langle s\rangle}$
	σ_{sy}^2	$1.5\langle y\rangle$	$0.75\langle y\rangle$	$1.5\frac{\tau_s\langle y\rangle}{\tau_y}$
$\tau_s \ll \tau_x$	Fano factor	$1+\frac{\langle y\rangle}{\langle x\rangle}+\frac{(\rho+3\frac{\tau_s}{\tau_x})\langle y\rangle}{\langle x\rangle}$	$1+0.5\frac{\langle y\rangle}{\langle x\rangle}+2.5\frac{\tau_s\langle y\rangle}{\tau_x\langle s\rangle}$	$1+\frac{\tau_x\langle y\rangle}{\tau_y\langle x\rangle}+4\frac{\tau_s\langle y\rangle}{\tau_y\langle s\rangle}$
	σ_{sy}^2	$(1+\frac{\tau_s}{\tau_x})\rho\langle y\rangle$	$(1+\frac{\tau_s}{\tau_x})\frac{\tau_s\langle y\rangle}{\tau_y}$	$(1+\frac{\tau_s}{\tau_x})\frac{\tau_s\langle y\rangle}{\tau_y}$

and co-variance of the target gene Y as

$$\sigma_y^2 = \langle y\rangle + \frac{\tau_y^{-1}\langle y\rangle^2}{(\tau_x^{-1}+\tau_y^{-1})\langle x\rangle} + \frac{\tau_y^{-1}\langle y\rangle^2}{(\tau_s^{-1}+\tau_y^{-1})\langle s\rangle} + \frac{3\tau_x^{-1}\tau_y^{-1}(\tau_s^{-1}+\tau_x^{-1}+\tau_y^{-1})\langle y\rangle^2}{(\tau_s^{-1}+\tau_x^{-1})(\tau_x^{-1}+\tau_y^{-1})(\tau_s^{-1}+\tau_y^{-1})\langle s\rangle},$$
$$\sigma_{sy}^2 = \frac{\tau_y^{-1}\langle y\rangle}{(\tau_s^{-1}+\tau_y^{-1})} + \frac{\tau_x^{-1}\tau_y^{-1}\langle y\rangle}{(\tau_s^{-1}+\tau_x^{-1})(\tau_s^{-1}+\tau_y^{-1})}. \quad (18)$$

It is interesting to note that for both TSC and ACFFL, we get almost equivalent variance expression (see Eq. (12) and Eq. (18)) except for two factors. These extra terms are the third and the fourth term on the right hand side of Eq. (18). The third term arises due to direct regulation of Y by S. The fourth term is multiplied by a numerical factor 3. From these extra terms, it is obvious that ACFFL shows higher fluctuating property than TSC due to the additive nature of two positive regulatory pathways (both direct and indirect) [2, 20, 63–65]. From Eq. (18), we get all possible reduced forms of Fano factor and co-variance expressions using nine possible relations among the three relaxation time scales (see Table IV).

As shown in the calculation for previous motifs, it is clear from Table IV that, for ACFFL, Fano factor and co-variance achieve maximum, intermediate and minimum values for $\tau_s \gg \tau_x \gg \tau_y$, $\tau_s \approx \tau_x \approx \tau_y$ and $\tau_s \ll \tau_x \ll \tau_y$, respectively. At these time scales, the modified forms of both Fano factor and co-variance are almost similar with the modified forms of TSC (see Table II) but terms like $\langle y\rangle/\langle s\rangle$ and $\langle y\rangle$ appear with multiplicative factor greater than 1. This leads to a high level of fluctuating environment for the ACFFL motif. The main reason behind the elevation of output fluctuations is the addition of fluctuations due to input signal S into the total fluctuations of the output component Y in two ways, direct and indirect pathways. Due to the such types of fluctuations addition phenomena, we get a higher Fano factor value. Similarly, we also obtain high level of mutual information $\mathcal{I}(s,y)$ transduction due to the presence of two subsequent pathways by which the target gene reliably accumulates signal information with greater extent and transcribes gene products precisely with the variation of input signal. To verify these features, we show Fano factor and mutual information as a function of relaxation rate constant τ_y^{-1} for four different parameter sets of relaxation rate constants in Fig. 5.

In Fig. 5(a), highest Fano factor value is obtained for the parameter sets $\tau_s^{-1} = \tau_x^{-1}/10 = 0.1$ and $\tau_s^{-1} = \tau_x^{-1}/100 = 0.1$. Both sets are due to faster fluctuations of the intermediate component X. On the other hand, lowest Fano factor value is attained for $\tau_s^{-1}/100 = \tau_x^{-1} = 0.1$ and is due to faster fluctuations of input signal S. For $\tau_s^{-1} = \tau_x^{-1} = 0.1$, the motif shows an intermediate Fano factor value. In all cases, Fano factor value increases with the relaxation rate constant of the target gene Y. Similar trend is also observed for the mutual information $\mathcal{I}(s,y)$ profile (Fig. 5(b)). Therefore, this motif has high information processing capacity in spite of the presence of high level of fluctuations. Such high input signal processing phenomena facilitate the networks reliability for signal transduction in GTRN and makes this motif a highly abundant one among rest of the CFFL present within the family of cellular networks. In this connection, it is important to mention that the network architecture can facilitate cellular fitness advantage in adverse environment due to increase of fluctuations. Thus, high

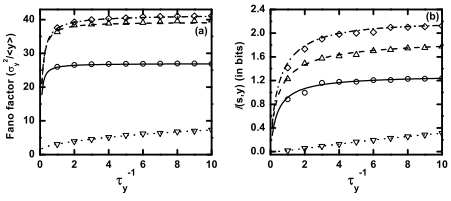

FIG. 5. The ACFFL. (a) Fano factor and (b) mutual information $\mathcal{I}(s,y)$ profiles as a function of relaxation rate constant τ_y^{-1} of Y component. The relations $k_1/\tau_s^{-1} = k_2/\tau_x^{-1} = 10$ and $k_3/\tau_y^{-1} = 0.1$ are maintained so that steady state population of all the components remain unaltered. In both plots, for solid (with open circles), dashed (with open upward triangle), doted (with open downward triangle) and dash dotted (with open diamond) lines we have used $\tau_s^{-1} = \tau_x^{-1} = 0.1$, $\tau_s^{-1} = \tau_x^{-1}/10 = 0.1$, $\tau_s^{-1}/100 = \tau_x^{-1} = 0.1$ and $\tau_s^{-1} = \tau_x^{-1}/100 = 0.1$, respectively. The symbols are generated using stochastic simulation algorithm [55, 56] and the lines are due to theoretical calculation.

fluctuations in output gene expression trigger phenotypic heterogeneity in clonal cell populations and can induce drug resistance [25, 66]. A similar type of CFFL is also liable for drug resistance of human cancer cells.

D. Incoherent feed forward loop

The last motif considered in the present work is another class of FFL known as Incoherent feed forward loop. We focus only on the type-1 incoherent feed forward loop (ICFFL) (Fig. 1(f)). In this motif, two regulatory pathways act in an opposite manner. Here, input signal S positively regulates the target gene Y through the direct pathway. However, the intermediate component X represses the expression of Y. As a result, S initially activates both X and Y rapidly but after some time, population level of X reaches a threshold to repress the production of Y. While modeling the repression phenomenon, we consider the Hill coefficient to be one. Thus, the Langevin equations for the dynamical quantities can be written as

$$\frac{dx}{dt} = k_2 s - \tau_x^{-1} x + \xi_x(t), \tag{19}$$

$$\frac{dy}{dt} = k_3 g(x) s - \tau_y^{-1} y + \xi_y(t). \tag{20}$$

In the above equation, $g(x) = K/(K+x)$ is a nonlinear repressive function that depends on the concentration of X and K, the ratio of unbinding to binding rate constants of transcription factor X at the promoter region of Y gene. We also consider $\langle g(x)s\rangle = \langle g(x)\rangle\langle s\rangle$ as the kinetic equations for both S and X are uncorrelated with each other and $\langle x\rangle/(K+\langle x\rangle) \approx 1$ as steady state concentration of the X component is much higher than the unbinding-binding constant ($x \gg K$). For this motif, we use the earlier kinetic equation for S (see Eq. (7)). Solving the set of kinetic equations, we get the simplified mathematical form of variance and co-variance [42–46]

$$\begin{aligned}\sigma_y^2 &= \langle y\rangle + \frac{\tau_y^{-1}\langle y\rangle^2}{(\tau_x^{-1}+\tau_y^{-1})\langle x\rangle} + \frac{\tau_y^{-1}\langle y\rangle^2}{(\tau_s^{-1}+\tau_y^{-1})\langle s\rangle} \\ &\quad - \frac{\tau_x^{-1}\tau_y^{-1}(\tau_s^{-1}+\tau_x^{-1}+\tau_y^{-1})\langle y\rangle^2}{(\tau_s^{-1}+\tau_x^{-1})(\tau_x^{-1}+\tau_y^{-1})(\tau_s^{-1}+\tau_y^{-1})\langle s\rangle}, \\ \sigma_{sy}^2 &= \frac{\tau_y^{-1}\langle y\rangle}{(\tau_s^{-1}+\tau_y^{-1})} - \frac{\tau_x^{-1}\tau_y^{-1}\langle y\rangle}{(\tau_s^{-1}+\tau_x^{-1})(\tau_s^{-1}+\tau_y^{-1})}. \end{aligned} \tag{21}$$

In the above variance expression, two S dependent fluctuations terms are present with opposite sign thus compensating each other. The variance expression is quite similar to the expression of TSC (see Eq. (12)) but differs in the sign of the last term and the appearance of an extra term due to direct regulation of Y by S. If one calculates the magnitude of variance for both TSC and ICFFL using unique steady state population level of all three components and the corresponding relaxation time scale, a higher value of σ_y^2 will be observed for TSC compared to ICFFL. To check the validity of this effect, we consider all possible relations among the three relaxation times of the corresponding network components and get nine possible relations. Using these relations, modified forms of Fano factor and co-variance are calculated and are given in Table V. From these modified expressions, it is clear that ICFFL exerts lesser amount of fluctuations compared to the other motifs considered in this work while developing the target gene product Y. Development of low fluctuations thus gets reflected in the Fano factor value. This happens due to repression of target gene by X which effectively reduces fluctuations associated with Y [2, 20, 63–65]. It is important to note that, in Table V, under some relaxation time scale limits, the Fano factor expressions are free from terms with $\langle s\rangle$, the S dependent fluctuations. This happens due to a simultaneous contribution of direct and indirect pathways which cancel each other by having equal magnitude but opposite sign. As a consequence, some of the co-variance values also become zero. This suggests that at these time scale limits, the system cannot incorporate the information of the input signal properly, thereby transducing information about the input signal unreliably to the target gene. Keeping this in mind, we explore the nature of Fano factor and mutual information $\mathcal{I}(s,y)$ as a function of relaxation rate constant τ_y^{-1} of Y component using four different sets, i.e., $\tau_s^{-1} = \tau_x^{-1} = 0.1$, $\tau_s^{-1} = \tau_x^{-1}/10 = 0.1$, $\tau_s^{-1}/100 = \tau_x^{-1} = 0.1$ and $\tau_s^{-1} = \tau_x^{-1}/100 = 0.1$.

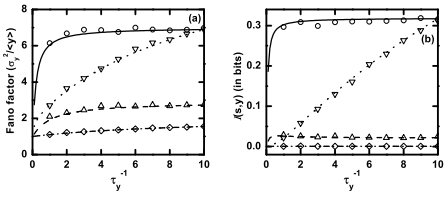

FIG. 6. The ICFFL. (a) Fano factor and (b) mutual information $\mathcal{I}(s,y)$ profiles as function of relaxation rate constant τ_y^{-1} of Y component. $k_1/\tau_s^{-1} = k_2/\tau_x^{-1} = 10$ and $k_3/\tau_y^{-1} = 1010$, ratios are maintained throughout these plots, so steady state population of all the components remain unaltered. In both plots, for solid (with open circles), dash (with open upward triangle), dot (with open downward triangle) and dash dot (with open diamond) lines, we use the following sets of parameters: $\tau_s^{-1} = \tau_x^{-1} = 0.1$, $\tau_s^{-1} = \tau_x^{-1}/10 = 0.1$, $\tau_s^{-1}/100 = \tau_x^{-1} = 0.1$ and $\tau_s^{-1} = \tau_x^{-1}/100 = 0.1$, respectively. The symbols are generated using stochastic simulation algorithm and the lines are from theoretical calculation.The symbols are generated using stochastic simulation algorithm [55, 56] and the lines are due to theoretical calculation.

In Fig. 6(a), Fano factor value gradually increases with the relaxation rate constant τ_y^{-1}. Very low level of Fano factor value is attained by the motif for $\tau_s^{-1} = \tau_x^{-1}/10 = 0.1$ and $\tau_s^{-1} = \tau_x^{-1}/100 = 0.1$. For these two sets, input fluctuations flow successfully through the direct and indirect pathways. Thus, two S dependent fluctuating terms that are equal in magnitude but opposite in sign compensate each other, consequently suppressing the fluctu-

TABLE V. Modified form of the analytical solution (Eq. (21)) of ICFFL motif. Fano factor ($\sigma_y^2/\langle y\rangle$) and co-variance ($\sigma_{sy}^2$) at different relaxation time limits are shown where $\rho = \tau_s/(\tau_s+\tau_y) \leqslant 1$.

		$\tau_x \gg \tau_y$	$\tau_x \approx \tau_y$	$\tau_x \ll \tau_y$
$\tau_s \gg \tau_x$	Fano factor	$1+\frac{\langle y\rangle}{\langle x\rangle}$	$1+0.5\frac{\langle y\rangle}{\langle x\rangle}$	$1+\frac{\tau_x\langle y\rangle}{\tau_y\langle x\rangle}$
	σ_{sy}^2	0	0	0
$\tau_s \approx \tau_x$	Fano factor	$1+\frac{\langle y\rangle}{\langle x\rangle}+0.5\frac{\langle y\rangle}{\langle s\rangle}$	$1+0.5\frac{\langle y\rangle}{\langle x\rangle}+\frac{\langle y\rangle}{8\langle s\rangle}$	$1+\frac{\tau_x\langle y\rangle}{\tau_y\langle x\rangle}$
	σ_{sy}^2	$0.5\langle y\rangle$	$0.25\langle y\rangle$	$0.5\frac{\tau_s\langle y\rangle}{\tau_y}$
$\tau_s \ll \tau_x$	Fano factor	$1+\frac{\langle y\rangle}{\langle x\rangle}+\frac{(\rho-\frac{\tau_s}{\tau_x})\langle y\rangle}{\langle s\rangle}$	$1+0.5\frac{\langle y\rangle}{\langle x\rangle}+0.5\frac{\tau_s\langle y\rangle}{\tau_y\langle s\rangle}$	$1+\frac{\tau_x\langle y\rangle}{\tau_y\langle x\rangle}$
	σ_{sy}^2	$(1-\frac{\tau_s}{\tau_x})\rho\langle y\rangle$	$(1-\frac{\tau_s}{\tau_x})\frac{\tau_s\langle y\rangle}{\tau_y}$	$(1-\frac{\tau_s}{\tau_x})\frac{\tau_s\langle y\rangle}{\tau_y}$

ations associated with the network. On the other hand, for the other two parameter sets, a high level of Fano factor values is found. This happens due to slower rate of fluctuations in the intermediate X. The input fluctuations that come through the indirect pathway are filtered out by X for its low pass filter nature. As a result, two S dependent fluctuating terms do not completely cancel each other. In these parameter sets, the fluctuating part that contributes to the direct pathway shows its prominent effect than the fluctuations due to indirect pathway which finally gets reflected in the total output fluctuations. Likewise, in Fig. 6(b), mutual information $\mathcal{I}(s,y)$ values are near to zero for the first two parameter sets giving low level of Fano factor and significant $\mathcal{I}(s,y)$ values for the rest of the parameter sets.

IV. CONLUSION

In this paper, we have analyzed signal transmission of a fluctuating input signal through highly specialized biochemical signaling networks. We have analytically calculated Fano factor of output and mutual information between input and output signals for two linear and three branched cascades to comprehend the significance of these networks in biological systems. On the basis of linear noise approximation, we have solved nonlinear chemical Langevin equations and verified the results with exact stochastic simulation of the corresponding nonlinear networks and found that the approximation method is quite accurate. In the analytical calculation, we have considered that all noise terms (ξ_s, ξ_x, ξ_y) are Gaussian in nature and the effect of cross correlation between two noise terms is zero. We have calculated Fano factor and mutual information for five networks with the variation of relaxation rate constants of all network components and have studied effect of input signal on these two measurable quantities. Our study not only takes care of individual motifs but also presents a comparative study of all the network motifs while considering Fano factor and mutual information. For graphical presentation of the output component of each motif, we have tuned synthesis and relaxation rate constant of each network components in such a way so that the steady state population of the network components remains constant as well as the total population of any network is also preserved. Adoption of such a policy helps us to apprehend how Fano factor and mutual information values get affected from one motif to another under equal population of network components.

We have started our calculations considering linear type of cascades and the first motif we have considered is OSC where the motif can precisely characterize the information of input signal at faster relaxation time of the output component compared to the input one. This accuracy gradually decreases with the increment of input relaxation rate. We have also shown that the OSC motif is unable to differentiate the variation of input signal at high population limit of input component. We then compare this motif with the standard gene regulation network to explicate such time scale effect on gene regulation and found some significant circumstances in which the gene regulatory network can tune up optimum fluctuations for both essential and nonessential proteins. Our analysis is at par with the results of Fraser et al [60] where they have performed analysis using several experimentally determined gene regulation rates.

The second motif TSC is then considered by introducing an intermediate component in OSC. Through our analysis, we have observed that Fano factor of output gets amplified in magnitude. In addition, similar kind of relaxation time scale effect for propagation of fluctuations as observed in OSC, is also present in this motif. Our analysis suggests that relaxation time scale of intermediate component is a crucial factor for signal transmission through this motif and can control fluctuations associated with the output. The intermediate component acts as a low pass filter for very fast fluctuations and hinders input fluctuations that flow through the TSC motif. After analyzing the TSC, we have introduced n number of intermediate components in between the input and the output component to generate a generalized linear long chain cascade and derived simplified form of Fano factor expression at three distinct time scale limits. We have shown that the output fluctuations increase with number of intermediate components and this result agrees with previously published several experimental and theoretical results. The main utility of these expressions is that one can easily calculate fluctuations associated with

any linear long chain cascade without enough knowledge of the parameter values of the network.

Next, we have chosen FFL, a group of branched pathways that are abundant in the signal transduction machinery of living systems and are generated by lateral combination of OSC and TSC with different modes of interaction. At first, we have studied OCFFL from FFL group and calculated Fano factor and mutual information with the extent of direct (OSC) and indirect (TSC) contribution of input signal to the target gene. In our calculation of Fano factor, we have observed two opposing behavior while tuning the control parameter. In one case, Fano factor decreases slowly while in the other situation, it shows an increasing trend. These results together suggest that OCFFL performs differently for diverse relaxation time scale limits. Furthermore, depending on the contribution of the direct and the indirect pathway, it can acquire the character of OSC and TCF motif, respectively. Such quality of OCFFL helps a living system to survive in diverse environmental conditions. We then extend our analysis to ACFFL where a high value of Fano factor and mutual information is observed. Such high values of Fano factor and mutual information reveals that ACFFL motif can transduce the signal with high reliability and supports its ubiquitous presence in several biological species. The last motif we have considered is ICFFL where output fluctuations are suppressed as the target gene is simultaneously regulated negatively (via indirect pathway with TSC character) as well as positively (via direct pathway with OSC character) by the input signal. This leads to a very low value of Fano factor and mutual information for ICFFL motif. Such low value suggests that living system containing this motif faces minimum fluctuations with low mutual information propagation.

To conclude, we emphasize that our methodology is very much general and is applicable for other network motifs under single cell environment. At this point, it is important to mention that enough single cell data are not available for FFL. Our theoretical results thus can act as a starting point to verify the stochastic nature of the network motifs we have considered in the present work. The nature of the results we have predicted can be tested by performing experiment in a single cell scenario. We expect that our work will influence several experimentalists in the coming days to understand the single cell behavior of these network motifs.

ACKNOWLEDGMENTS

We thank Debi Banerjee for critical reading of the manuscript. AKM and PC are thankful to University Grants Commission, New Delhi, for research fellowship (UGC/776/JRF(Sc)) and for a major research project, respectively. SKB acknowledges financial support from CSIR, India [01(2771)/14/EMR-II] and Bose Institute (through Institutional Programme VI - Development of Systems Biology).

[1] U. Alon, *An Introduction to Systems Biology: Design Principles of Biological Circuits* (CRC Press, 2006).
[2] U. Alon, Nat Rev Genet **8**, 450 (2007).
[3] A. L. Barabási and Z. N. Oltvai, Nat Rev Genet **5**, 101 (2004).
[4] R. Milo, S. Shen-Orr, S. Itzkovitz, N. Kashtan, D. Chklovskii, and U. Alon, Science **298**, 824 (2002).
[5] J. J. Tyson, K. C. Chen, and B. Novak, Curr Opin Cell Biol **15**, 221 (2003).
[6] C. J. Marshall, Cell **80**, 179 (1995).
[7] J. M. Robison and H. M. Cobb, Curr Opin Cell Biol **9**, 180 (1997).
[8] R. Heinrich, B. G. Neel, and T. A. Rapoport, Mol Cell **9**, 957 (2002).
[9] M. T. Laub and M. Goulian, Annu Rev Genet **41**, 121 (2007).
[10] N. E. Hynes, P. W. Ingham, W. A. Lim, C. J. Marshall, J. Massagué, and T. Pawson, Nat Rev Mol Cell Biol **14**, 393 (2013).
[11] T. I. Lee, N. J. Rinaldi, F. Robert, D. T. Odom, Z. Bar-Joseph, G. K. Gerber, N. M. Hannett, C. T. Harbison, C. M. Thompson, I. Simon, et al., Science **298**, 799 (2002).
[12] S. S. Shen-Orr, R. Milo, S. Mangan, and U. Alon, Nat Genet **31**, 64 (2002).
[13] A. Blais and B. D. Dynlacht, Genes Dev **19**, 1499 (2005).
[14] L. A. Boyer, T. I. Lee, M. F. Cole, S. E. Johnstone, S. S. Levine, J. P. Zucker, M. G. Guenther, R. M. Kumar, H. L. Murray, R. G. Jenner, et al., Cell **122**, 947 (2005).
[15] H. Jeong, B. Tombor, R. Albert, Z. N. Oltvai, and A. L. Barabási, Nature **407**, 651 (2000).
[16] N. C. Duarte, S. A. Becker, N. Jamshidi, I. Thiele, M. L. Mo, T. D. Vo, R. Srivas, and B. Ø. Palsson, Proc Natl Acad Sci U S A **104**, 1777 (2007).
[17] J. Förster, I. Famili, P. Fu, B. Ø. Palsson, and J. Nielsen, Genome Res **13**, 244 (2003).
[18] J. D. Han, N. Bertin, T. Hao, D. S. Goldberg, G. F. Berriz, L. V. Zhang, D. Dupuy, A. J. Walhout, M. E. Cusick, F. P. Roth, et al., Nature **430**, 88 (2004).
[19] U. Stelzl, U. Worm, M. Lalowski, C. Haenig, F. H. Brembeck, H. Goehler, M. Stroedicke, M. Zenkner, A. Schoenherr, S. Koeppen, et al., Cell **122**, 957 (2005).
[20] M. Kaern, T. C. Elston, W. J. Blake, and J. J. Collins, Nat Rev Genet **6**, 451 (2005).
[21] R. Losick and C. Desplan, Science **320**, 65 (2008).
[22] F. J. Bruggeman, N. Blüthgen, and H. V. Westerhoff, PLoS Comput Biol **5**, 1 (2009).
[23] M. Kittisopikul and G. M. Süel, Proc Natl Acad Sci U S A **107**, 13300 (2010).
[24] E. Rotem, A. Loinger, I. Ronin, I. Levin-Reisman, C. Gabay, N. Shoresh, O. Biham, and N. Q. Balaban, Proc Natl Acad Sci U S A **107**, 12541 (2010).
[25] D. A. Charlebois, N. Abdennur, and M. Kaern, Phys Rev Lett **107**, 218101 (2011).

[26] B. Munsky, G. Neuert, and A. van Oudenaarden, Science **336**, 183 (2012).
[27] J. P. Armitage, Adv Microb Physiol **41**, 229 (1999).
[28] M. Thattai and A. van Oudenaarden, Biophys J **82**, 2943 (2002).
[29] S. Hooshangi, S. Thiberge, and R. Weiss, Proc Natl Acad Sci U S A **102**, 3581 (2005).
[30] J. M. Pedraza and A. van Oudenaarden, Science **307**, 1965 (2005).
[31] S. Tănase-Nicola, P. B. Warren, and P. R. ten Wolde, Phys Rev Lett **97**, 068102 (2006).
[32] S. Mangan and U. Alon, Proc Natl Acad Sci U S A **100**, 11980 (2003).
[33] J. Tsang, J. Zhu, and A. van Oudenaarden, Mol Cell **26**, 753 (2007).
[34] B. Ghosh, R. Karmakar, and I. Bose, Phys Biol **2**, 36 (2005).
[35] F. Hayot and C. Jayaprakash, J Theor Biol **234**, 133 (2005).
[36] R. Murugan, PLoS One **7**, 1 (2012).
[37] U. Fano, Phys. Rev. **72**, 26 (1947).
[38] A. Borst and F. E. Theunissen, Nat Neuroscience **2**, 947 (1999).
[39] P. Mehta, S. Goyal, T. Long, B. L. Bassler, and N. S. Wingreen, Mol Syst Biol **5**, 325 (2009).
[40] A. A. Faisal, L. P. Selen, and D. M. Wolpert, Nat Rev Neurosci **9**, 292 (2008).
[41] W. H. de Ronde, F. Tostevin, and P. R. Ten Wolde, Phys Rev E **86**, 021913 (2012).
[42] J. Elf and M. Ehrenberg, Genome Res **13**, 2475 (2003).
[43] P. S. Swain, J Mol Biol **344**, 965 (2004).
[44] W. Bialek and S. Setayeshgar, Proc Natl Acad Sci U S A **102**, 10040 (2005).
[45] N. G. van Kampen, *Stochastic Processes in Physics and Chemistry* (North-Holland, Amsterdam, 2005).
[46] W. H. de Ronde, F. Tostevin, and P. R. ten Wolde, Phys Rev E **82**, 031914 (2010).
[47] C. E. Shannon, Bell Syst Tech J **27**, 379 (1948).
[48] T. M. Cover and J. A. Thomas, *Elements of Information Theory* (Wiley interscience, 1991).
[49] M. B. Elowitz, A. J. Levine, E. D. Siggia, and P. S. Swain, Science **297**, 1183 (2002).
[50] P. S. Swain, M. B. Elowitz, and E. D. Siggia, Proc Natl Acad Sci U S A **99**, 12795 (2002).
[51] J. M. Raser and E. K. O'Shea, Science **304**, 1811 (2004).
[52] J. Paulsson, Nature **427**, 415 (2004).
[53] A. Hilfinger and J. Paulsson, Proc Natl Acad Sci U S A **108**, 12167 (2011).
[54] M. Scott, B. Ingalls, and M. Kaern, Chaos **16**, 026107 (2006).
[55] D. T. Gillespie, J Comp Phys **22**, 403 (1976).
[56] D. T. Gillespie, J Phys Chem **81**, 2340 (1977).
[57] M. Thattai and A. van Oudenaarden, Proc Natl Acad Sci U S A **98**, 8614 (2001).
[58] E. M. Ozbudak, M. Thattai, I. Kurtser, A. D. Grossman, and A. van Oudenaarden, Nat Genet **31**, 69 (2002).
[59] W. J. Blake, M. Kaern, C. R. Cantor, and J. J. Collins, Nature **422**, 633 (2003).
[60] H. B. Fraser, A. E. Hirsh, G. Giaever, J. Kumm, and M. B. Eisen, PLoS Biol **2**, 0834 (2004).
[61] M. Thattai and A. van Oudenaarden, Genetics **167**, 523 (2004).
[62] A. Becskei, B. B. Kaufmann, and A. van Oudenaarden, Nat Genet **37**, 937 (2005).
[63] A. Raj and A. van Oudenaarden, Cell **135**, 216 (2008).
[64] A. Eldar and M. B. Elowitz, Nature **467**, 167 (2010).
[65] R. Silva-Rocha and V. de Lorenzo, Annu Rev Microbiol **64**, 257 (2010).
[66] D. A. Charlebois, G. Balázsi, and M. Kærn, Phys Rev E **89**, 052708 (2014).